Advances in CFD Modelling of Multiphase Flows in Cyclone Separators

Dimitrios Papoulias*[a], Simon Lo[b]

[a]CD-adapco, 200 Shepherds Bush Road, London, W6 7NL, UK
[b]CD-adapco, Trident House, Basil Hill Road, Didcot, OX11 7HJ, UK
dimitrios.papoulias@cd-adapco.com

This paper evaluates the predictive performance of modern Computational Fluid Dynamics (CFD) methods in cyclone vortex-separation flows. Computer simulations are performed with the Eulerian-Eulerian (E-E) as well as Eulerian-Lagrangian (E-L) multiphase models, available is STAR-CCM+ CFD solver. Tested momentum closure strategies included typical two-equation isotropic turbulence models as well as high-order Reynolds Stress Models (RSM) and Large Eddy Simulation (LES) technique. The calculated results show satisfactory agreement compared to corresponding Laser Doppler Velocimetry (LDV) measurements and experimental values for the separation efficiency (η).

1. Introduction

Centrifugal fluid-flow devices are widely used in the industry for the segregation of multiphase flow-mixtures into their constituent fluid components. Over years in operation, flow cyclones have been continuously scrutinized in order to gain understanding of the underlying fluid-flow mechanics and their effects in the separation efficiency of fluid/solid mixtures. The research studies published by Colman et al. (1980), Thew et al. (1984) and Svarovskyet et al. (1992) encapsulate much of the experimental work done in hydrocyclones, mainly used for oil refinery processes. Results presented in these reports were primarily concerned with the migration probability of oil-droplets – the decontamination of the carrier water fluid – as a function of the operation conditions i.e. Reynolds number (Re), loading volume-fractions (vf) and droplet-size populations. In some cases, the cyclonic vortex-flow was accessed with LDV inspection techniques (Bai et al., 2009); this allowed full characterization of the vortex flow, in terms of the mean and fluctuating velocity components, for different flow-rates and at different sections of the model. Similar experimental studies have also been published in gas-solid cyclones and swirling tubes (Hoekstra, 2000), typically used in chemical and catalyst manufacturing plants as well as the food industry.

The results obtained using the aforementioned experimental methods in cyclone flows generated an extensive database of measurements and test-conditions, useful for developing and validating CFD models. To overcome the inherited limitations of early analytical methods and mechanistic models (Gomez, 2001), flow engineers pursued CFD models based on the Navier-Stokes (NS) equations. Computer predictions using the Lagrangian-particle model are presented and validated in the work of Derksen (2003), against LDV measurements provided in Stairmand's gas-solid cyclone (Stairmand, 1951). The Eulerian-Eulerian multiphase approach is adopted in the study of Slot (2013), for the evaluation of the deoiling process in hydrocyclone separation regimes. Recently, hybrid CFD techniques are also developed which combine optimization models coupled with two-phase flow solvers, in an attempt to derive high-efficiency cyclone geometries (Sgrott et al., 2013). In order to capture the highly anisotropic and mixing character of two-phase vortex flows in cyclones, most of the aforesaid studies employed high-order turbulence models, despite the overhead computational costs. The significance of turbulent effects in the development of confined vortex flows gradually shifted research in this topic from the traditional Reynolds-Averaged NS models (RANS) to LES techniques.

The work presented is this paper is concerned with the performance of RANS and LES CFD solution techniques for predicting cyclonic flows. A brief description of two-phase RANS solution models is given in the next section.

2. CFD models for multiphase flows

The dynamic motions of dispersed phases in a continuous carrier flow can be modelled either by adopting the two-fluid E-E realization or by considering the discrete E-L approach. In the latter case, the dispersed phase is simulated by tracking the individual trajectories of discrete particle populations, while in the former method the flow phases coexist in time and space as interpenetrating continua. The averaged RANS equations in the context of Eulerian and Lagrangian multiphase flow models are formulated as:
continuity:

$$\frac{\partial}{\partial t}(a_i \rho_i) + \nabla(a_i \rho_i u_i) = 0 \tag{1}$$

momentum:

$$\frac{\partial}{\partial t}(a_i \rho_i u_i) + \nabla(a_i \rho_i u_i u_i) = -a_i \nabla p + a_i \rho_i g_i + \nabla a_i \tau_i + F_i \tag{2}$$

In addition to Eq. (1), the volume-fractions of the multiphase flow must also sum to unity:

$$\sum_{j \neq i} a_j = 1 \tag{3}$$

where α is the volume-fraction, u is the velocity, ρ the density, p the pressure, g the gravitational acceleration and the index i denotes the individual flow phases.
In the E-L model, the momentum balance (Eq. 2) for the dispersed-phase is redeveloped to a trajectory equation for the motion of the discrete homogeneous parcels:

$$\sum F_i = m_p \frac{du_p}{dt} \tag{4}$$

where m_p is the mass of the travelling particle (e.g. droplet, solid-particle).
Closure of the system of equations requires supplementary models for approximating the flow forces F and the turbulent stresses τ, acting between the different phases. Contributions in the force-vector term accounted for flow effects due to drag F_D, lift $F_{L,S}$, virtual-mass $F_{V,D}$ and turbulent dispersion $F_{T,D}$.
For realizing the effective eddy-diffusivity of turbulent two-phase flows, different turbulence models can be used. Usually, this part of the flow is treated with two-equation isotropic turbulence models, therefore adopting the Boussinesq approximation for the eddy viscosity. This reduces the problem to two transport equations, one for the turbulent kinetic-energy k and one for its dissipation rate ε. On the other hand, RSM methods account for the directional sense of each of the individual turbulent stresses, as a function of the local pressure-strain as well as the rotation of the flow. RSM models restore the anisotropy of turbulent eddies at the expense of six extra differential transport-equations. For increasingly complex flows the aforementioned RANS CFD models are not always successful. Numerical methods which developed to cope with such situations, are designed to resolve rather than model the length and time scales of mixing eddies. The principle behind these techniques is the decomposition of the instantaneous flow-field into large-scale and sub-grid contributions, by applying an LES filter. Modelling of the unresolved part – the small-scale dissipating eddies – is performed with the so-called Smagorinsky sub-grid scale model (SGS). Based on the eddy-viscosity assumption, SGS models provide the turbulence stresses of the traceless part, needed for closure, as a function of the strain-tensor and the grid-size filter Δ. Mathematical formulations and modelling details regarding the aforementioned turbulence models are covered in the work of Launder et al. (2002).
The turbulent multiphase models described in this section are tested for different parametric flows in cyclone separators; the simulated boundary conditions and the geometric details of the examined cyclone models are discussed in the forthcoming paragraphs.

3. Parametric single-phase and multiphase simulations in cyclones

The CFD simulation scenarios performed in this work covered different modelling aspects of cyclonic flows. In details the tested solution models and flow conditions are summarized in Table 1. Information regarding the design, boundary types and the discretized physical solution domain are illustrated in Figure 1.

Starting from the top of Table 1, the first-set of validation simulations engaged the E-E multiphase method in order to replicate the flow behaviour of a single-phase gas cyclone (Figure 1 a), using two identical fluids. Parametric tests for this case examined the solution effects of different turbulence models and multiphase volume-fractions for realizing the continuous gas flows. The results from this study are compared against available LDV measurements, which captured the mean flow-field at different spatial locations (Figure 3). The second series of simulations in Table 1, examined Stairmand's cyclone model (Figure 1 b) for single-phase flow conditions as well as for two-phase gas-solid mixing regimes, using the E-L solver. Single-phase calculations demonstrated the usefulness of the LES method in this types of flows, while the two-phase runs simulated the interactions developing between the mean flow and particles of different sizes (D_p=1-10 µm). As in the previous cases, the obtained predictions are validated against corresponding LDV experimental results (Figure 4) and measured values for the collection efficiency ($m_{out,i}/m_{in,i}$). The third case listed in Table 1 is concerned with multiphase validation calculations performed in Colman's oil-water hydrocyclone (Figure 1 c). In this example, both the E-E and E-L models are employed for predicting the separation of the two-phase flow, as a function of different oil-droplet sizes (D_p=20-100 µm). For benchmarking purposes the obtained calculations are plotted alongside to equivalent experimental values for the grade efficiency of the dilute oil phase (Figure 5).

Table 1: Parametric simulation cases; solution models and flow conditions.

Cyclone model	Solution grid	Multiphase model	Turbulence model	Boundary conditions	Flow phase(s) volume-fractions
1) Stairmand (without bin)	0.6M to 1M poly &hexa	E-E	k-ε & RSM	U_{in}= 20 m/s p_{out} = 1 bar	air-air: 50% - 50% air-air: 20% - 80%
2) Stairmand (with collection bin)	7M hexa	E-L	RSM & DES	U_{in}= 20 m/s p_{out} = 1 bar	solid: 1.0%
3) Colman	13M hexa	E-E & E-L	RSM	U_{in}= 6 m/s p_{out} = 1 bar	oil: 1.0%

In all cases the solution domain is discretized with fine hexahedral cells, ranging from 0.6M to 13M elements. The properties of the working air, oil and water fluids are taken in standard state conditions. The results of the undertaken parametric study in cyclone flows are analyzed and discussed in the next sections.
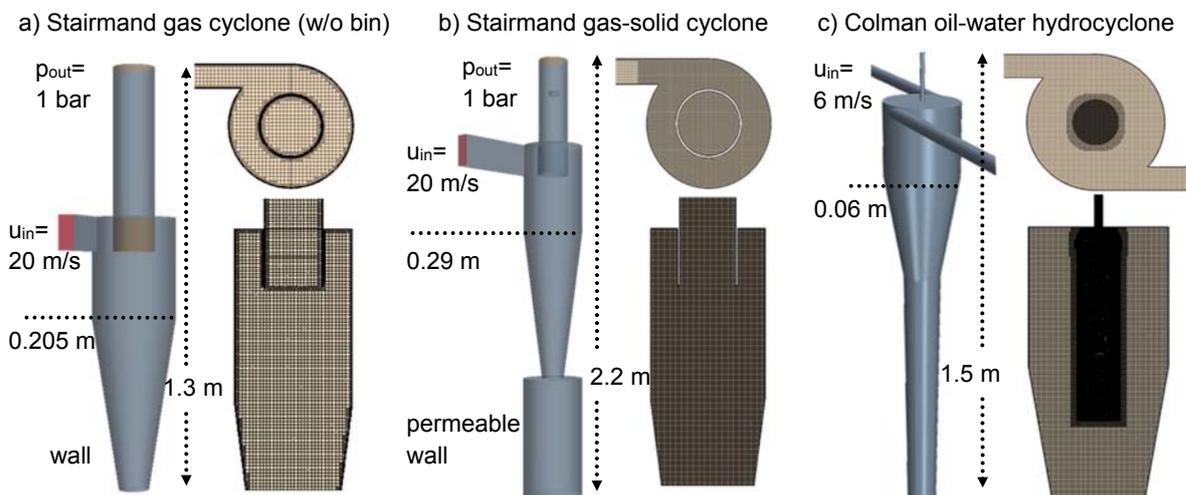
a) Stairmand gas cyclone (w/o bin)   b) Stairmand gas-solid cyclone   c) Colman oil-water hydrocyclone

Figure 1: Cyclone models; geometric characteristics, discretized solution domain and boundary conditions.

4. CFD Results

The first test-case studied in this report analysed the vortex-flow developing inside a modified gas cyclone, based on Stairmand's design. In this model the downstream collection bin is removed and instead the cyclone is sealed with a wall boundary (Figure 1 a). Results from this case are shown in Figure 2 and Figure 3. The behaviour of the vortex gas-flow inside Stairmand's cyclone is realized by looking at the instantaneous

1606

pressure field, developing at different time-steps (Figure 2). Apparently, the core of the forming vortex inside the cyclone swings from side to side, following a transient 'dancing' motion.
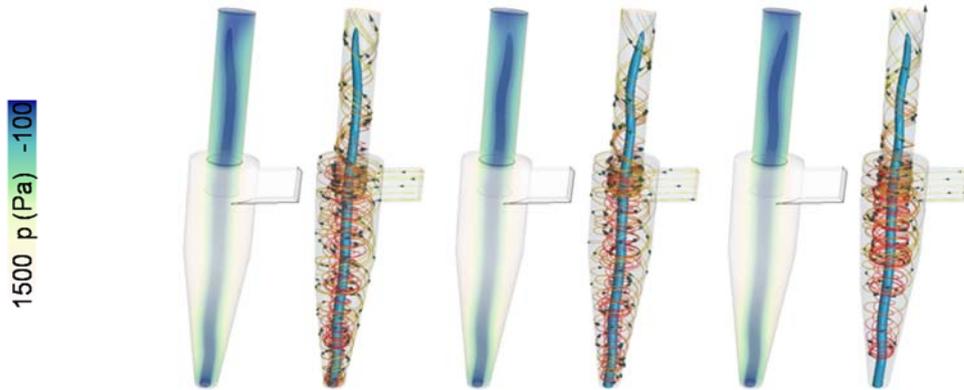

Figure 2: Instantaneous single-phase flow solution-steps; scenes showing volume-rendered pressure-drop contours and recirculating flow streamlines in the vortex-core region (iso-surface).

Despite the fact that this problem can be effectively treated as steady-state, the unsteady nature of this flow is also evident from the mean flow contours and spatial LDV plots shown in Figure 3. Instead in this case the flow was iterated for 3 s – in steps of 1 ms – and the mean solution was averaged over a period of 2 s. The resulting time-averaged velocity-profiles (Figure 3 b) indicated the decay of the vortex-flow as it evolves further downstream (z=0.59 m), and more importantly exposed solution sensitivities to turbulence modelling. Overall, the RSM predictions appear to capture the development of the vortex flow, both at locations where the flow swirl is at peak levels (z=0.32 m) but also further downstream where part of the recirculation degenerates to small-eddies at the walls. On the contrary, the two-equation realizable turbulence model (RLZ) appears rather diffusive, especially as the flow converges towards the sealed-exit at the bottom of the cyclone (z=0.59 m). Satisfactory results are also predicted when the multiphase E-E RSM technique is used in order to mimic the single-phase flow. In this case the gas-phase is substituted by two identical fluids, assuming different vf concentrations. The velocity distributions calculated for the latter parametric tests displayed excellent agreement with the respective single-phase results and LDV measurements, irrespective of the input vf analogy for representing the equivalent phases.
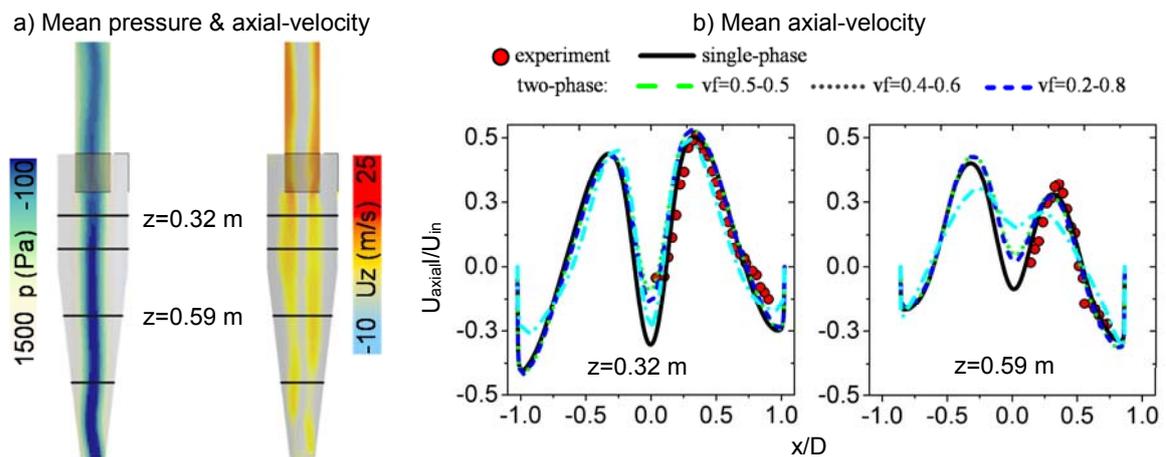

Figure 3: Time-averaged flow results; contours showing mean pressure and axial-velocity variables and plots of the spatial velocity distribution at different sections superimposed with LDV measurements.

Flow calculations for Stairmand's cyclone are presented in Figure 4. This part of the analysis is mainly focused on the separation dynamics of solid particles as it occurs inside the vortical gas flow. The two-phase flow is simulated using the one-way coupled E-L model, given that the concentration of the particle-phase accounts only for 1 % of the total vf. The background single-phase flow, which serves for extrapolating information at each parcel location, is time-averaged over a simulation period of 3 s. For these transient calculations the

RSM approach is pursued in conjunction with a second-order upwind scheme. In addition, the LES model is also tested for single-phase flow conditions. The predictions provided by the LES method appear to be remarkably close to the LDV measurements for the mean tangential velocity (Figure 4 a). The dynamic response of the solid-particles in this type of flow is illustrated in Figure 4 b. In these contour plots the predicted relative positions and trajectories of discrete particles are shown, for different diameter sizes. As expected, larger particles seem to accumulate inside the collection bin, while particles with smaller diameters are captured in the vortex core and carried towards the top exit. According to experiments (Hoekstra, 2000), the separation efficiency of the two-phase mixing regime is measure to be 25.7 % (D_p=10 µm) and 100.0 % (D_p=1 µm) respectively. The respective values predicted by the E-L particle solver are 24.3 % and 99.9 %.

a) LES Single-phase flow; mean tangential velocity
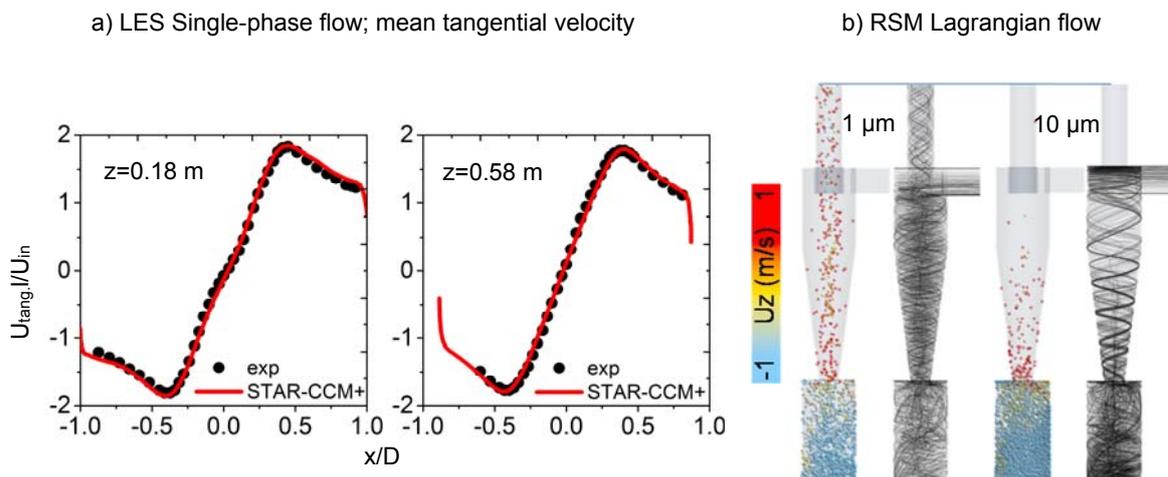
b) RSM Lagrangian flow

Figure 4: Spatial mean tangential velocity profiles superimposed with LDV results and particle trajectories.

Two-phase flow simulations in Colman's hydrocyclone, using the one-way coupled E-L model as well as the E-E two-fluid approach are presented in Figure 5. In this case, the multiphase mixture consists mainly of water and low-concentrations of oil droplets, 1 % by volume. As done in the previous Lagrangian calculations, the continuous liquid flow is uncoupled from the dispersed phase; instead the integration of the droplet trajectories is calculated over the time-averaged solution of the liquid phase. The E-E simulations are treated as time-dependant, fully-coupled calculations. In both case, turbulence effects are resolved with the RSM model.

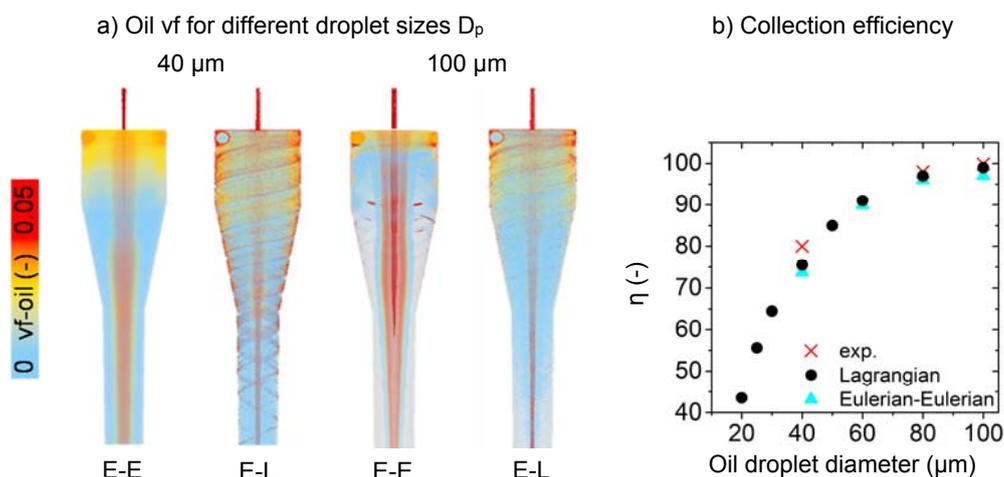a) Oil vf for different droplet sizes D_p

b) Collection efficiency

Figure 5: Two-phase Eulerian and Lagrangian flow calculations; scenes showing volume-rendered contours of the dispersed oil phase volume-fraction and plots of the predicted separation efficiency superimposed with corresponding experimental measurements.

In Colman's cyclone, the oil and water fluids enter the domain tangentially from the two side inlets at a speed of 6 m/s. Separation of the mixture begins when the flow is promoted to a fully developed vortex. The suction

of the vortical flow captures the larger droplets, which get trapped inside the low-pressure core. Smaller droplets manage to escape the attraction of the vortex and continue their journey downstream, following the decelerated flow near the wall. This situation is confirmed by the E-E and E-L model predictions as illustrated in Figure 5 a. Looking at the way the flow is distributed inside the cyclone it becomes apparent that the lighter oil fluid prefers to live mainly at the vortex core region. The heavier water component exists at the periphery of the vortical eye, which eventually is discharged at bottom clean exit of the cyclone. Effective decontamination of the oil depleted water occurs when the oil droplets increase in size (100 μm). This behaviour is also confirmed by the calculated values of the separation efficiency (Figure 5 b). In fact, both models indicated an asymptotic rise of the separation efficiency, for increasing droplet diameter sizes. Compared to the experimental results, both multiphase solution techniques appear to be satisfactory accurate.

5. Conclusions

In this study parametric single-phase and two-phase flow calculations were performed in different cyclone separator models, using the STAR-CCM+ CFD solver. The predicted cyclone flow-field revealed the formation of transient vortex structures, which frequently performed cyclic oscillations. Time-averaged calculations using the RSM and LES methods matched accurately LDV measurements of the tangential and axial velocity variations of the unsteady vortex flow, at different spatial locations. On the contrary, isotropic turbulence models diffused the extent and the rotational speed of the developing cyclone vortex. Calculated multiphase results regarding the separation efficiency of the tested cyclone geometries were also found to be consistent with corresponding experimental values and in agreement between the E-E and E-L solvers. Overall, the utilized CFD techniques proved to be a valuable design tool for resolving turbulence characteristics, vortex mixing dynamics and particle-flow interactions in internal cyclone flows, under different operation conditions.

References

Bai Z.-S., Wang H.-L., 2009, Experimental study of flow patterns in deoiling hydrocyclones, Mineral Engineering, 22(4), 319-323.

Colman D.A., Thew M.T., Corney D.R., 1980, Hydrocyclones for oil/water separation, Proc. Int. Conference on hydrocyclones, paper 11, 143-165, 1-3 October 1980, Churchill College, Cambridge, UK.

Derksen J.J., 2003, Separation performance predictions of a Stairmand high-efficiency cyclone, AIChE Journal, 49(6), 1359-1371.

Gomez C.H., 2001, Oil-water separation in liquid-liquid hydrocyclones (LLHC) - Experiments and Modelling, M.S. Thesis, University of Tulsa, United States.

Hoekstra A.J., Derksen A.J, Van Den Akker H.E.A., 1999, An experimental study of turbulent swirling flow in gas cyclones, Chemical Engineering Science, 54, 2055-2065.

Hoekstra A.J., 2000, Gas flow field and collection efficiency of cyclone separators, PhD thesis, Delft University of Technology, The Netherlands.

Launder B.E., Sandham N.D, Eds., 2002, Closure Strategies for Turbulent and Transitional Flows. Cambridge University Press, United Kingdom.

Sgrott Jr O. L., Costa K. K.., Noriler D., Wiggers V. R., Martignoni W. P., Meier H. F., 2013, Cyclones' project optimization by combination of an inequality constrained problem and computational fluid dynamics techniques (CFD), Chemical Engineering Transactions, 32, 2011-2016.

Svarovsky L., Thew M.T, Eds., 1992, Hydrocyclones Analysis and Applications. Springer-Science and Business Media, Letchworth, England.

Stairmand C.J., 1951, The design and performance of cyclone separators, Transactions Chemical Engineering, 29, 356-383.

Slot J.J., 2013, Development of a centrifugal in-line separator for oil-water flows, PhD thesis, University of Twente, The Netherlands.

Thew M.T., Wrighy C.R., Colman D.A., 1984, Characteristics of hydrocyclones for the separation of light dispersions, Proc. 2nd Int. Conference on hydrocyclones, 163-176, 17-20 September 1984, Bath UK.